3in1: Multi-tone Joint Powering, Clocking, and Communication for Passive IoT

Ruirong Huang
Johns Hopkins University
Baltimore, Maryland, USA
rhuang36@jhu.edu

Renjie Zhao
Johns Hopkins University
Baltimore, Maryland, USA
rjzhao@jhu.edu

Abstract

Passive IoT technology, valued for its self-sustaining and low-cost attributes, faces notable limitations in data rate, range, and power efficiency. While significant progress has been made in enhancing uplink performance through backscattering techniques, the primary performance bottleneck has now shifted to the downlink. In this paper, we propose *3in1*, a novel multi-tone system that jointly optimizes wireless power delivery, high-precision clocking, and robust communication for long-range passive IoT devices. By carefully controlling the phase and frequency spacing of the multi-tone signals, *3in1* significantly improves energy harvesting efficiency, seamlessly provides wireless clocking, and enables reliable downlink communication without interrupting power transfer. Our design addresses critical challenges, including signal optimization, data encoding, and strict FCC compliance.

We implement *3in1* using a software-defined radio (SDR)-based transmitter and a custom-built passive tag. Real-world experiments with our prototype demonstrate a 6× increase in power conversion efficiency, a 3× extension in operational range (up to 22 m), and a 19× reduction in cold-start time compared to the Gen2 UHF RFID protocol. Simultaneously, *3in1* delivers a clock signal with zero offset at 2 MHz and < 1 ns jitter, along with a high-speed 200 kbps downlink achieving a bit error rate (BER) below 10^{-3}—all while remaining fully compliant with FCC regulations. This work represents a significant advance in passive IoT, enabling efficient, long-range, and practical deployments in real-world environments.

CCS Concepts

• **Hardware → Wireless devices**.

Keywords

Wireless Power Transfer, Wireless Clocking, Multi-Tone BPSK

ACM Reference Format:
Ruirong Huang and Renjie Zhao. 2026. *3in1*: Multi-tone Joint Powering, Clocking, and Communication for Passive IoT. In *ACM/IEEE International Conference on Embedded Artificial Intelligence and Sensing Systems (SenSys '26), May 11–14, 2026, Saint Malo, France.* ACM, New York, NY, USA, 14 pages. https://doi.org/10.1145/3774906.3800458

1 INTRODUCTION

Due to its self-sustaining, maintenance-free, and low-cost characteristics, passive IoT technology holds transformative potential across a wide range of applications. Among these technologies, radio-frequency identification (RFID) is the most widely adopted, with extensive use in inventory management, asset tracking, and access control [58, 62]. However, conventional RFID systems suffer from low data rates, limited operating ranges, and high infrastructure costs, which hinder broader deployment in scenarios such as real-time environmental monitoring, large-scale smart agriculture, and ubiquitous sensing for smart homes and cities [24].

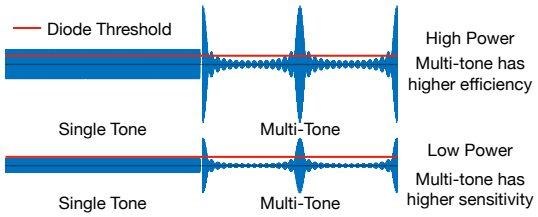

(a) With the same average power, multi-tone has better WPT efficiency and sensitivity.

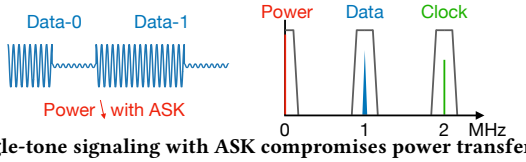

(b) Single-tone signaling with ASK compromises power transfer efficiency, whereas *3in1*'s multi-tone signal embeds both clock and data within the beat frequencies, ensuring uninterrupted and efficient power delivery.

Figure 1: Comparison Between Widely Adopted Single-tone and Multi-tone in *3in1*

To address these limitations, extensive research has explored long-range, high-data-rate backscatter communication for the uplink [10, 20, 30, 61, 63]. However, these designs often overlook the challenges associated with wireless power delivery and downlink performance. Specifically, RF energy harvesters typically require input signals stronger than −20 dBm to generate even microwatt-level output power [56], in contrast to the −90 dBm receiver sensitivity achievable by uplink gateways [29]. This significant difference in sensitivity results in a substantial range gap: while uplink communication can reach distances up to kilometers [49], wireless power delivery is typically limited to around 10 m. As for the downlink communication, while sub-microwatt wake-up receivers have been demonstrated [34, 35], their circuit simplicity limits modulation to amplitude shift keying (ASK), reducing power transfer efficiency due to lower average power. As a result, ***downlink*** performance—including both powering and communication—remains the primary ***bottleneck*** of passive IoT.

Moreover, unlike conventional RFID systems that utilize sub-MHz clocks with tolerances up to 20%—readily achievable using

SenSys '26, Saint Malo, France

ACM ISBN 979-8-4007-2309-4/2026/05
https://doi.org/10.1145/3774906.3800458

sub-microwatt open-loop oscillators—recent backscatter designs often require highly accurate clocks operating in the several-to-tens of MHz range [10, 20, 30, 61, 63]. Meeting these stringent frequency requirements necessitates closed-loop clock generators with crystal references, which significantly increases cost and power consumption (by one to two orders of magnitude), and leads to additional energy waste due to oscillator stabilization delays [20, 44]. These requirements contradict the foundational design principles of passive IoT. Consequently, many existing designs rely on battery support [25, 28, 41, 42, 64], which undermines the low-maintenance advantage of passive IoT, or operate at very short ranges (under 5 meters) when powered solely by wireless means [12, 14, 44], limiting their practical utility.

To deal with these problems, there have been separate studies on improving power transfer efficiency and sensitivity through high peak-to-average power ratio (PAPR) signals [11, 13, 15, 16, 18, 26, 36, 38, 46, 52–54], enabling long-range low-power downlink communication [25], and providing clocks wirelessly [1, 2, 44], most of these design principles are in conflict with one another. As a result, there is currently no unified solution that addresses all the downlink challenges simultaneously. This raises a fundamental question: **Is it possible to design a downlink waveform that can simultaneously and efficiently provide wireless powering, accurate clocking, and robust communication?**

To address this question, we propose *3IN1*, the first multi-tone system that jointly optimizes wireless powering, clocking, and communication for long-range passive IoT devices. The key insight underpinning *3IN1* is that multi-tone signals offer two significant advantages, as illustrated in Fig. 1:
i) Power efficiency and sensitivity: By generating a high peak-to-average power ratio (PAPR) signal, *3IN1* improves both energy harvesting efficiency and sensitivity. This is achieved by increasing the proportion of signal energy that exceeds the diode-based harvester's forward voltage threshold.
ii) Clock and communication: When tones are evenly spaced, the non-DC (AC) components of the harvested signal become concentrated at beat frequencies between the tones. These frequency components, which are not rectified into DC energy, can be repurposed for wireless clocking and data transmission, thereby enabling robust and accurate downlink communication without interrupting power transfer—in contrast to ASK-based single-tone designs, which compromise energy delivery when modulating data.

However, achieving joint optimization through multi-tone signal design entails overcoming several critical challenges:

How can we design the multi-tone signal to optimize power delivery and wireless clocking? The phase differences between tone components in a multi-tone signal significantly influence its envelope shape, [1] directly impacting power delivery efficiency [17]. Therefore, precise signal design is crucial for maximizing efficiency. Since performance depends not only on the transmitted signal but also on the energy harvester's response, we theoretically analyze the conditions necessary to achieve the highest PAPR in a multi-tone signal and model its effect on energy harvesting efficiency. We prove that the maximum PAPR is attained when the phase differences between all adjacent tones remain uniform and that energy harvesting efficiency improves as the number of tones increases. Additionally, under these optimal conditions, the extracted clock signal strengthens with more tones, ensuring reliable wireless clocking.

How can we introduce data communication without degrading power delivery or distorting the clock? Amplitude-based modulation, like that used in UHF RFID, allows ultra-low-power (ULP) decoding but reduces average power during communication, making power delivery the limiting factor for passive IoT. To overcome this, we propose a downlink communication scheme that preserves both power and clock integrity. By revisiting the constraints identified in the first challenge, we observe that tuning the phase shift between adjacent tones enables data encoding without compromising power efficiency. Specifically, by adjusting the phase difference between odd and even tone components between 0 and π—implementing a multi-tone BPSK scheme—we achieve the design illustrated in Fig. 7. This approach encodes data at the fundamental frequency while preserving the second harmonic as a phase-stable clock (alternating between 0 and 2π).

How can we integrate everything into a practical system? Bringing this design into a real-world system introduces three additional challenges: *(i) Trade-off in the number of tones:* While increasing the number of tones improves power efficiency and clock strength, excessive tones create two issues. First, a high PAPR signal requires a high-linearity, high-power amplifier (PA) which is very costy. Second, maintaining a sufficient downlink data rate requires a minimum tone spacing of 500 kHz. Too many tones would result in an excessively wide bandwidth, complicating regulatory compliance and practical implementation. Considering these constraints, we select a 16-tone signal with 1 MHz spacing as the optimal balance between performance and feasibility. *(ii) Receiver design for passive IoT:* Unlike existing designs that require separate circuits for different downlink functions [44, 59], our system enables power, data, and clock extraction using a single envelope detector, which simultaneously serves as a rectifier and a mixer. To ensure seamless extraction of each component without interference, we propose a joint filter design that enables parallel signal processing. *(iii) FCC regulation:* Unlike single-tone narrowband signals, our multi-tone design occupies a much wider bandwidth and must comply with FCC 47 CFR 15.247 (a)(2) and (e) [22], which limit power spectral density to 8 dBm per 3 kHz. However, when transmitting at the maximum allowed 30 dBm power for extended range, a native 16-tone signal would yield approximately 18 dBm per tone ($30 + 10\log_{10}(\frac{1}{16}) \approx 18$), exceeding the 8 dBm regulatory limit. To address this, we leverage the fact that carrier frequency does not impact the signal after envelope detection. We implement a frequency-hopping mechanism across 100 channels to distribute power, ensuring FCC compliance while preserving power delivery, clocking, and communication integrity.

We implement *3IN1* using an SDR-based transmitter and a custom PCB-based passive tag. Extensive experiments evaluate *3IN1* across various scenarios, including multi-tone configurations, input power levels, channel fading, operating range, and tag cold-start time. Real-world experiments demonstrates significant performance gains, including a 6× improvement in power conversion efficiency, 3× increase in operating range, and 19× faster cold-start time compared

[1] This effect has been widely studied in reducing PAPR or crest factor to enhance power amplifier efficiency [27]. However, our objective is to deliberately increase PAPR to improve downlink performance.

Table 1: Comparing *3IN1* with previous works.

Systems	Wireless Powering	Wireless Clocking	Downlink Communication	Other Limitations
Powering Only [11, 13, 16, 17]	*ICW, UWB, Chaotic, Noise,* Multi-Tone	—	—	*Crystal & No Downlink Data*
Clocking Only [1, 2]	—	*Two-Tone Beat Frequency*	—	*Battery & No Downlink Data*
Downlink Only [28, 35, 41, 64]	—	—	*OOK, QAM, BPSK*	*Battery & Crystal*
Powering & Downlink [3, 12, 21, 33, 45, 57, 59]	Multi-Tone , *Single-Tone*	—	*ASK*	*Crystal*
Powering & Clocking [7]	*Single-Tone*	*Single-Tone Injection Locking*	—	*No Downlink Data*
3IN1	**Phase-Controlled Multi-Tone**	**Multi-Tone Beat Frequency**	**Multi-Tone BPSK**	**No**

to the Gen2 UHF RFID protocol. Simultaneously, *3IN1* delivers a clock signal with zero offset at 2 MHz and < 1 ns jitter, along with a high-speed 200 kbps downlink achieving a bit error rate (BER) below 10^{-3}—all while remaining fully compliant with FCC regulations.

The key contributions of this work are:

- We propose the first multi-tone system that jointly optimizes wireless powering, clocking, and communication.
- We analyze how to jointly optimize the performance while handling multiple practical challenges in multi-tone system adoption.
- We develop a hardware prototype of the transmitter and passive tag, demonstrating significant downlink performance improvements in powering, clocking, and communication across various real-world scenarios.

2 MOTIVATION AND RELATED WORKS

As shown in Table. 1, although prior work has explored wireless powering, wireless clocking, and downlink communication individually, no existing design integrates and optimizes all three into a unified system. As a result, many IoT tags still rely on batteries [25, 28, 41, 42, 64], and many require an on-tag crystal oscillator to generate an accurate clock, increasing cold-start time, power consumption, and tag cost [20, 44]. Furthermore, most passive IoT downlink designs rely on ASK or OOK modulation [3, 12, 21, 33–35, 45, 57, 59], which reduces signal amplitude and thus compromises wireless power transfer efficiency. These dependencies on batteries and crystals, along with the limited operating range, remain key bottlenecks for passive IoT systems.

2.1 Wireless Power Transfer

Wireless Power Transfer (WPT) has long relied on single-tone Countinous Wave (CW) signal [59], which has poor Power Conversion Efficiency (PCE) on rectifier side [11]. Some studies explored beamforming to enhance power delivery at specific spatial locations [21, 57]. However, this inherently reduces WPT efficiency in other locations, limiting scalability. Additionally, determining the precise location of battery-free tags presents a chicken-and-egg problem: the tags need to respond to provide location feedback, yet they may lack sufficient power to do so.

Recent research has investigated high PAPR signals for WPT, including multi-tone, random signals, UWB, intermittent CW, white noise, etc. [11, 13, 16, 17]. However, most of these approaches remain theoretical due to hardware complexity, lack of robustness, or FCC compliance issues. Some efforts [3, 33] have leveraged multi-tone signals to enhance WPT efficiency, but their phase alignment was not optimized. Studies [12, 14, 52] have demonstrated that in-phase multi-tone waveforms improve the operating range of UHF RFID systems. However, their downlink communication still relies on ASK, which compromises power transfer efficiency.

In contrast, *3IN1* optimizes the starting phase condition for PAPR-enhanced multi-tone waveforms and employs BPSK, which preserves WPT efficiency while enabling robust downlink communication.

2.2 Wireless Clocking

[1, 2] investigated using a two-tone signal to wirelessly distribute an accurate clock with low Clock Frequency Offset (CLKFO) and jitter, enabling coherent transmission among wireless nodes. However, these methods require a complicated high-power receiver which is not suitable for passive IoT. Moreover, they suffer from a key robustness issue—if one of the two tones is lost, clock extraction fails, and their waveform design is incompatible with downlink communication, as modulation would distort the clock signal.

[7] proposed extracting a clock from a 900 MHz UHF RFID downlink using harmonic injection locking and frequency division by three to generate a 300 MHz clock. However, 300 MHz is too high for passive IoT tag, leading to increased power consumption. Moreover, it does not support frequency hopping, as the fixed division ratio restricts adaptability.

In contrast, *3IN1* employs beat frequencies of a multi-tone waveform for wireless clocking, offering greater flexibility in frequency adjustment and improved robustness against channel fading.

2.3 Downlink Communication

To simplify demodulation on battery-free IoT devices, current downlink modulation schemes are predominantly ASK or OOK [34, 35, 59]. However, amplitude-based modulation inherently sacrifices wireless power delivery by reducing signal strength for communication. To mitigate this issue, the UHF RFID protocol incorporates pulse interval encoding (PIE) before applying ASK for downlink modulation, where during 50% of a data-0 symbol and 30% of a data-1 symbol, the CW amplitude is reduced to just 10% of its maximum value. Consequently, the delivered power drops to 1% or even lower, considering the power conversion efficiency loss in Schottky diode rectifiers.

Other IoT systems, such as LoRa, use frequency-shift spread spectrum for communication [6]. However, LoRa receivers are not ulra-low power, consuming tens to hundreds of milliwatts [19], which is far beyond what battery-free devices can afford. Additionally, LoRa's low Peak-to-Average Power Ratio (PAPR) results in suboptimal WPT efficiency. Current low-power BPSK receivers [5, 9, 23, 60] predominantly use non-coherent demodulation due to the high power consumption required to recover the carrier signal on the tag. However, this compromises receiver sensitivity and data rate.

Some studies have explored using two-tone signals for downlink communication, eliminating the need for Local Oscillator (LO) [28,

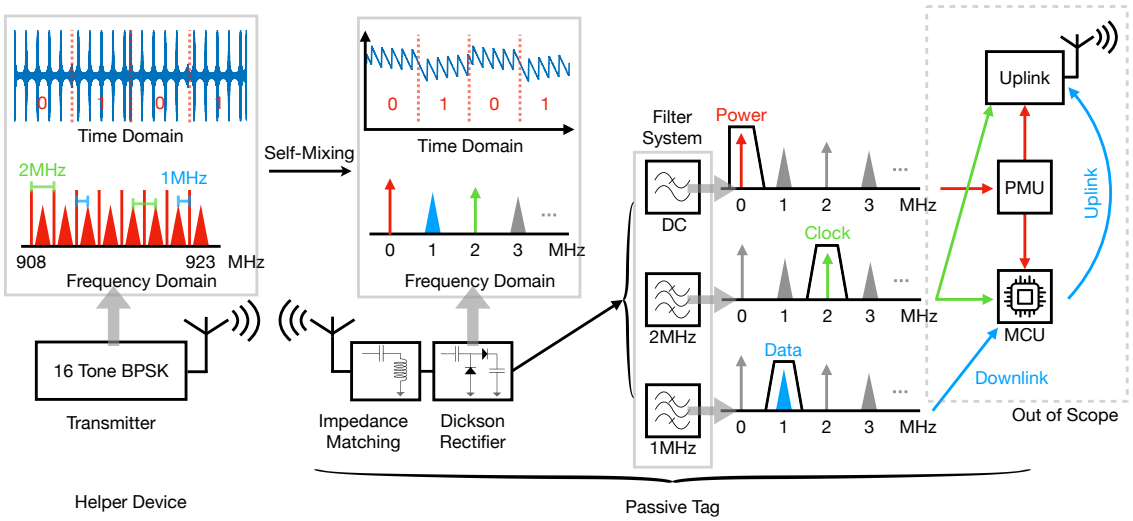

Figure 2: *3IN1* System Overview

41, 64]. However, their waveform designs are not optimized for WPT, requiring battery-powered tags. More recent passive IoT tag designs [45, 59] integrate power harvesting and communication, but they rely on separate branches for power harvesting and envelope detection, effectively cutting the harvested DC power in half.

In contrast, *3IN1* introduces a novel multi-tone BPSK modulation scheme that preserves signal amplitude. By encoding downlink data in the relative phase between adjacent tones, it enables seamless coexistence with wireless clocking, which is embedded in the beat frequency between alternate tones. As a result, power, clock, and data are integrated into a unified and optimized multi-tone waveform. Furthermore, *3IN1* employs a single rectifier on the tag and separates the different frequency components afterward, maximizing DC power harvesting while reducing tag complexity and cost.

3 OVERVIEW

As illustrated in Fig. 2, the *3IN1* design consists of a helper device that wirelessly delivers power, clock, and data communication using an optimized multi-tone signal, and a passive tag that harvests power while extracting clock and data. The multi-tone signal comprises 16 evenly spaced tones with 1 MHz frequency separation. In its default state, all tones have an initial phase of 0, maximizing efficiency and sensitivity for both power transfer and clocking (Sec. 4).

For downlink communication, the tones are divided into two groups based on their index parity. The even-indexed tones undergo BPSK modulation by shifting their initial phase between 0 and π, enabling data transmission without compromising power delivery or clocking (Sec. 5).

The passive tag features a single rectifier that simultaneously harvests energy and acts as a mixer, extracting beat frequencies between tones for clock and data recovery. A filtering system then separates power, clock, and downlink data from the rectifier output (Sec. 6). While the passive IoT tag should also include an ultra-low-power microcontroller unit (MCU), a power management unit (PMU), and an uplink modulation scheme, the optimization of these components is beyond the scope of this paper.

4 MULTI-TONE DESIGN

In this section, we will focus on how to design a multi-tone signal that can simultaneously enhance the sensitivity and efficiency of wireless powering and wireless clocking.

4.1 Power Delivery Optimization

4.1.1 Initial phase conditions for highest PAPR. As illustrated in Fig. 3, the waveform of a multi-tone signal varies significantly depending on its initial phase configuration. Consequently, the efficiency and sensitivity of different multi-tone signals also differ. Since a rectifier achieves higher efficiency and sensitivity at higher PAPR [17], it is crucial to determine the optimal starting phase configuration that maximizes PAPR.

Here, we first prove that for an equally spaced multi-tone signal $x(t)$ with N tones of same amplitude, the highest PAPR is achieved when a constant phase shift of $\Delta\phi$ exists between adjacent tones, satisfying the following condition:

$$\Delta\phi \frac{w}{\Delta w} = k\pi, k \in \mathbb{Z} \tag{1}$$

where w is the frequency of the first tone, Δw is the frequency difference between adjacent tones.

Proof. The time-domain representation of the signal is given by:

$$x(t) = \sum_{i=0}^{N-1} A_N \cos((w + i\Delta w)t + i\Delta\phi) \tag{2}$$

where

$$A_N = \frac{A}{\sqrt{N}} \tag{3}$$

is the amplitude of each tone in the multi-tone signal, and A represents the amplitude of a single-tone signal with the same average power. It is obvious that the signal in Eq. 2 reaches its maximum value when all tones peak simultaneously at a certain time t_0, i.e.

$$\cos((w + i\Delta w)t_0 + i\Delta\phi) \approx \pm 1, \forall i \in 0 \sim N-1 \tag{4}$$

which implies that

$$(w + i\Delta w)t_0 + i\Delta\phi = k_1\pi - \epsilon, \forall i \in 0 \sim N-1, k_1 \in \mathbb{Z} \tag{5}$$

where ϵ should be minimized to approach zero.

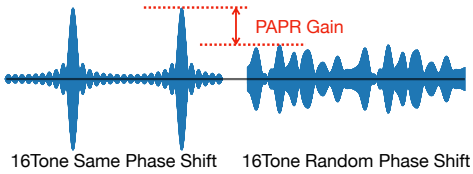

Figure 3: Multi-Tone with Same Phase Shift Between Nearby Tones Has Highest PAPR

Rearranging Eq. 5, we obtain:

$$wt_0 + i(\Delta w t_0 + \Delta\phi) = k_1\pi - \epsilon,\ \forall i \in 0 \sim N-1,\ k_1 \in \mathbb{Z} \quad (6)$$

To satisfy Eq. 6, the following conditions must hold:

$$\begin{cases} wt_0 = k_1\pi - \epsilon, \\ \Delta w t_0 + \Delta\phi = k_2\pi, \end{cases} \quad k_1, k_2 \in \mathbb{Z} \quad (7)$$

By substituting Eq. 1, we achieve $\epsilon = 0$, meaning that all tones align at their peak value at a specific time $t = t_0$. If Eq. 1 is not strictly satisfied, ϵ can still be minimized by selecting appropriate values for k_1, k_2, though it may not reach exactly zero. A straightforward choice that satisfies Eq. 1 is $\Delta\phi = 0$, meaning all tones start with the same phase (i.e., they are in-phase). In this case, the peak voltage of the multi-tone signal in Eq. 2 occurs at $t = 0$ of each period. Therefore, we select zero phase shift as the default waveform for power delivery and use the other phase shift in the design of downlink communication in Sec. 5.

4.1.2 More tones improves WPT efficiency. Next, we demonstrate that an in-phase multi-tone signal with more tones yields a higher DC voltage output. The nonlinear rectifier model, considering the two most significant parameters contributing to nonlinearity [17], is given by:

$$V(t) = k_2 x(t)^2 + k_4 x(t)^4 \quad (8)$$

where k_2, k_4 are positive model coefficients, $x(t)$ is the received signal, and $V(t)$ is the rectifier's output voltage. For an in-phase, uniformly spaced multi-tone waveform with N tones, the time-domain signal can be expressed as:

$$x(t) = \sum_{i=0}^{N-1} A_N \cos((w + i\Delta w)t) \quad (9)$$

By combining Eqs. 8, 9, and 3, the DC output voltage of the rectifier is:

$$\begin{aligned} V_{DC} =& \frac{Nk_2}{2}A_N^2 + \frac{N(2N^2+1)k_4}{8}A_N^4 \\ =& \frac{1}{2}k_2A^2 + \frac{2N^2+1}{8N}k_4A^4 \end{aligned} \quad (10)$$

This result clearly shows that WPT efficiency and sensitivity improve monotonically with the number of tones. Fig. 4 further illustrates this trend, demonstrating that an increased number of tones leads to a higher PAPR, thereby enhancing WPT efficiency.

4.2 Integrated Wireless Clocking

To ensure continuous power delivery and clock synchronization without compromising either, we co-design wireless clocking within the optimized WPT waveform. The multi-tone waveform inherently supports this by leveraging its beat frequencies to carry the clock signal. As illustrated in Fig. 5, when the multi-tone signal passes through a rectifier, it undergoes self-mixing, generating multiple

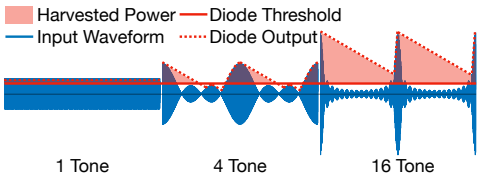

Figure 4: In-Phase 1, 4, 16 Tone Waveform with Same Average Power Passing Through a Diode

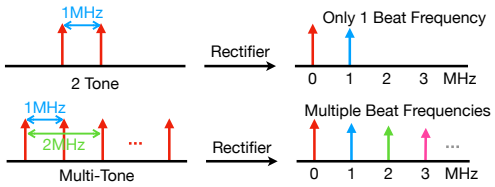

Figure 5: Beat Frequencies of 2-Tone and Multi-Tone

beat frequencies in the output. The number of these beat frequencies increases with the number of tones, enhancing the robustness and reliability of clock extraction.

4.2.1 More tones means higher clock voltage. Crucially, there is no trade-off between WPT efficiency and wireless clocking. This is because the approach effectively repurposes otherwise unused frequency components from the rectifier output without reducing the extracted DC voltage. Neglecting k_4 for simplicity, the extracted beat frequency voltage is given by:

$$V_{beat} = \sum_{i,j,i-j=1}^{1\le i,j\le N} k_2 A_N^2 = \frac{N-1}{N}k_2A^2 \quad (11)$$

which demonstrates a monotonic increase in voltage as the number of tones grows, confirming that power delivery and clocking do not compete with each other. The choice of beat frequency under practical constraints is discussed in Sec. 6.

4.2.2 Resiliance to multipath-rich indoor. The multi-tone approach also enhances robustness against frequency-selective fading caused by multipath effects, particularly as the number of tones increases. Unlike a two-tone signal, where losing a tone results in a missing clock signal, the evenly spaced multi-tone design ensures clocking remains intact even if some tones are lost.

This resilience stems from the fact that each beat frequency between tones is "down-converted" by the rectifier to the baseband, aligning with the desired clock frequency. As long as at least one copy of the beat frequency is received at the tag, the clock signal can still be successfully extracted. Additionally, since the extracted clock frequency at the receiver precisely matches the configured beat frequency at the transmitter, the system inherently achieves ultra-low Clock Frequency Offset (CLKFO) and minimal jitter.

5 DOWNLINK COMMUNICATION DESIGN

To optimize the co-design of downlink communication with power delivery and wireless clocking, we adopt phase shift keying (PSK), which maintains a constant amplitude. Unlike ASK, PSK preserves signal power and avoids frequency variations that could disrupt wireless clocking. However, integrating PSK within the multi-tone waveform presents two key challenges:

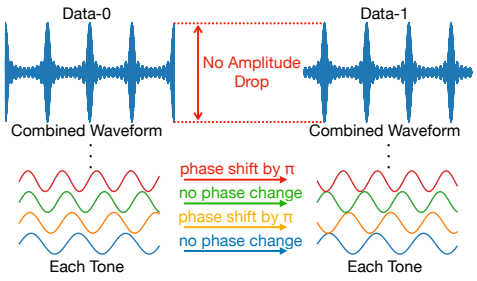

Figure 6: Multi-Tone BPSK Modulation

Figure 7: Multi-Tone BPSK Modulation Does Not Distort Wireless Clocking

5.1 How to Avoid Influencing Powering?

This challenge arises because the PAPR of a multi-tone signal is highly dependent on the relative phase between tones. Although applying a same phase shift across all tones might appear to be a simple and intuitive approach, it introduces significant complications for downlink data demodulation. This is because phase information after rectification primarily exists in the carrier frequency (above 900 MHz) or its harmonics, which are difficult to extract in an ultra-low-power manner.

To ensure that PSK-modulated data remains accessible on a passive IoT device, it must be embedded within the beat frequencies between tones. This way, after passing through the rectifier, the PSK data is naturally downconverted to the baseband, making it easy to extract. However, to maintain optimal power delivery, we must also satisfy the condition established in Sec. 4.1, where the phase difference between all adjacent tones must remain uniform, denoted as $\Delta\phi$. As illustrated in Fig.6, we can encode data by setting $\Delta\phi = 0$ for 0 and $\Delta\phi = \pi$ for 1. Notably, this scheme ensures that there is no amplitude drop when carrying different data symbols, preserving power delivery efficiency while enabling reliable downlink communication.

5.2 How to Avoid Distorting Clock?

Another key challenge is that arbitrarily switching between different $\Delta\phi$ can introduce sudden phase shifts across all beat frequencies, leading to distortion in wireless clocking. This brings us to the second major challenge: ensuring phase shifts do not degrade clocking stability.

We observe that setting $\Delta\phi = \pi$ introduces useful properties. While maintaining a uniform phase shift between adjacent tones —thereby preserving optimal power delivery—the phase shift between every other tone becomes 2π, effectively resetting to zero. This ensures that the beat frequencies formed between every other tone remain undistorted, allowing them to reliably support wireless clocking.

Building on this insight, we propose a novel multi-tone BPSK design that applies BPSK modulation to only half of the tones in an interleaved pattern. As illustrated in Fig. 6, for a Data-0 symbol, all tones maintain the same starting phase. For a Data-1 symbol, we introduce a π phase shift to even tones (e.g., the 2nd, 4th, 6th, ..., and 16th tones in a 16-tone signal).

After rectification, the downlink BPSK data is embedded within the beat frequencies between adjacent tones, while the wireless clocking remains encoded in the beat frequencies between every other tone, as shown in Fig. 7, where the straight line means no modulation on that tone, and a triangle means BPSK modulation on that tone.

This design preserves wireless clocking integrity for three reasons.

(1) The beat frequency between every other tone remains 2 MHz because the individual tone frequencies remain unchanged during modulation.
(2) There are no sudden phase transitions within the beat frequencies used for clocking. As illustrated in Fig. 7: (i) No modulation is applied between any two odd tones, ensuring phase continuity. (ii) While even tones undergo BPSK modulation and experience phase shifts, they are modulated simultaneously. As a result, no abrupt phase change occurs within the beat frequencies between any two even tones.
(3) Due to the properties of BPSK modulation, the second harmonic of the beat frequency remains phase-invariant. A π phase shift at the fundamental beat frequency translates to a 2π (or effectively 0) phase shift at its second harmonic, ensuring that even-order harmonics remain undistorted as shown in Fig. 8. Therefore, BPSK is a deliberate and necessary design choice, as higher modulation orders will inevitably distor the clock signal.

6 PUT *3IN1* TOGETHER UNDER PRACTICAL CONSTRAINTS

Bringing *3IN1* multi-tone design into a real-world system introduces three additional challenges:

6.1 Trade-off on Number of Tones

While increasing the number of tones improves power efficiency and clock strength, excessive tones create two issues.

(1) Too many tones will lead to a very high PAPR signal that requires a high-linearity power amplifier (PA) to send the multi-tone signal without large distortion. Considering that we want to send the high power signal for long-range operation, the needs of high-linearity high power PA will introduce unaffordable cost.
(2) To maintain a sufficient downlink data rate without interfering with the wireless clocking, the tone spacing must be much larger than the bandwidth of the downlink modulated signal. Then, too many tones result in an excessively wide bandwidth, making regulatory compliance and practical implementation challenging.

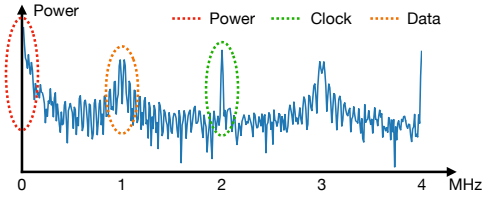

Figure 8: Spectrum after Rectifier: Even-order Harmonics Carry No Phase Shift

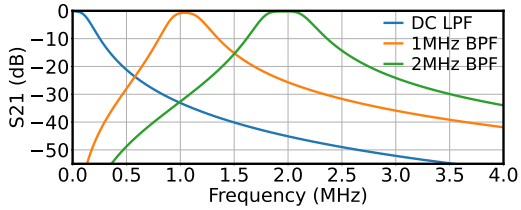

Figure 9: S21 of 3IN1's Filter System

Considering these constraints, we select a 16-tone signal with 1 MHz spacing as the optimal trade-off between performance and feasibility. The wireless clocking will be carried on the 2 MHz beat frequency between every other tones as shown in Fig. 8, which is a balance between uplink data rate and digital circuit power consumption.

6.2 Receiver Design

On the passive IoT side, we need to extract power, clock, data simultaneously in an ultra-low power fashion. To achieve this goal, we propose a novel receiver design (Fig. 2) that consists of a single rectifier and joint-optimized filter system.

6.2.1 Single rectifier. As discussed in Sec. 4.2 and 5, both clock and data extraction from the multi-tone signal rely on self-mixing. Since the rectifier used for DC power extraction also inherently performs self-mixing, its output simultaneously contains power, data, and clock signals, as illustrated in Fig.7. Leveraging this property, *3IN1* adopts a single rectifier design on the receiver side, ensuring a simple and fully passive implementation.

Notably, we use a one-stage Dickson voltage multiplier as the rectifier due to its full-wave rectification capability. While increasing the number of stages can boost the output DC voltage and improve sensitivity, it significantly degrades Power Conversion Efficiency (PCE) at lower input power levels [8]. To optimize the operating range of passive IoT devices, we prioritize a one-stage design. The final integration of *3IN1* into a passive IoT system should also account for PMU requirements to enhance overall system efficiency at the target sensitivity.

6.2.2 Filter system. To extract power, clock, and data from a single rectifier, a carefully designed filter system is required to separate these signals at DC, 2 MHz, and 1 MHz, respectively. The system consists of three parallel LC filters: (i) a Low-Pass Filter (LPF) that extracts DC for power harvesting, (ii) a Band-Pass Filter (BPF) centered at 2 MHz to recover the clock signal, and (iii) a BPF centered at 1 MHz to extract the BPSK data.

Designing this filter system is nontrivial because simply combining multiple LC filters can cause mutual distortion, shifting the resonance frequencies and degrading performance. Additionally, the bandwidth of each filter must be carefully selected—filters that are too narrow suffer excessive passband loss due to the limited Q-factor of practical LC components, while overly broad filters can cause interference between power, clock, and data.

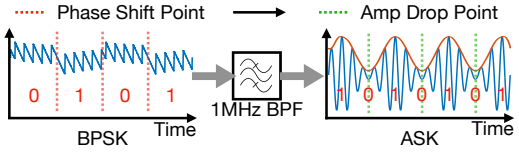

Figure 10: BPSK to ASK Conversion

To balance signal isolation and loss, we use a second-order Chebyshev filter for the BPFs and a first-order Chebyshev filter for the LPF. The 2 MHz BPF is designed with a 3 dB bandwidth of 0.4 MHz and provides 32 dB attenuation at 1 MHz to effectively isolate the clock signal from data interference. The 1 MHz BPF has a 3 dB bandwidth of 0.4 MHz, with 26 dB and 60 dB attenuation at 2 MHz and 100 kHz, respectively, ensuring that neither DC power extraction nor wireless clocking is compromised. The DC LPF provides 33 dB attenuation at 1 MHz, minimizing the impact on downlink communication sensitivity. The final frequency response of the filter bank is shown in Fig. 9.

6.2.3 BPSK to ASK conversion. The 1 MHz BPF also plays a crucial role in BPSK demodulation. Since BPSK modulation introduces sudden phase shifts, the signal's transient bandwidth momentarily expands during these shifts. As shown in Fig. 10, when the signal passes through a narrow BPF, the out-of-band frequency components are filtered out, causing a significant amplitude drop during phase transitions. This effect enables the BPF to effectively convert the BPSK-modulated signal into an ASK-like signal, which can be demodulated in an ultra-low-power manner.

Importantly, this process does not compromise WPT efficiency because: (i) DC power is extracted through the LPF branch and remains unaffected by the 1 MHz BPF, and (ii) the BPSK-to-ASK conversion is a fully passive process that requires no additional power consumption.

Furthermore, since the 2 MHz clock is derived from the same multi-tone signal through a single rectifier, it remains naturally in-phase with the downlink modulation. This synchronization enables coherent demodulation, which further enhances both the downlink data rate and sensitivity.

6.3 FCC Regulation

Unlike UHF RFID readers, which can transmit at 30 dBm under FCC 47 CFR 15.247(a)(1)(i) by utilizing frequency hopping, *3IN1*'s multi-tone signal occupies a much broader bandwidth and must comply with FCC 47 CFR 15.247(a)(2) as a digitally modulated signal [22]. Furthermore, FCC 47 CFR 15.247(e) imposes a maximum signal strength limit of 8 dBm within any 3 kHz bandwidth, presenting a challenge for our multi-tone waveform design.

Given that the average transmission power is set at the maximum allowed 30 dBm before the antenna, a straightforward 16-tone signal would allocate approximately 18 dBm per tone ($30 + 10\log_{10}(\frac{1}{16}) \approx 18$), which exceeds the 8 dBm FCC limit. To overcome this, we leverage the fact that the carrier frequency does not affect V_{DC} and beat frequencies after envelope detection as shown in Fig. 11. We

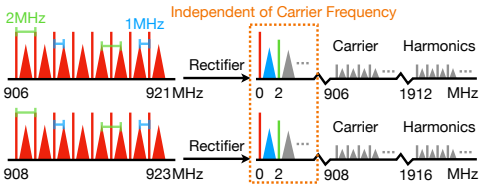

Figure 11: Baseband Signal after Rectifier is Independent of Carrier Frequency

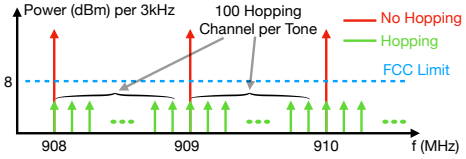

Figure 12: Frequency Hopping Illustration

implement a frequency hopping mechanism that preserves power, clock, and data integrity while adhering to FCC constraints. Specifically, we shift all 16 tones together 100 times within every 1-second interval, with each hop shifting by 10 kHz to avoid overlapping adjacent tones. As illustrated in Fig. 12, this technique distributes the originally concentrated signal energy across a wider spectrum, reducing peak signal strength by a factor of 100 (or 20 dB), ensuring compliance with the 8 dBm per 3 kHz FCC regulation. The effectiveness of this approach is demonstrated through experimental results in the evaluation section.

Note that the frequency hopping scheme is transparent to the tag. Since the carrier frequency is inherently down-converted to baseband during rectification, the tag's powering, clocking, and downlink communication functions remain unaffected by the hopping process.

7 IMPLEMENTATION

As shown in Fig. 13, we implement the prototype of both helper device and tag.

7.1 Transmitter

Note that this multi-tone BPSK waveform does not require specialized hardware. The phase-modulated multi-tone signal is fundamentally a simplified OFDM waveform, which can be efficiently generated using commercial off-the-shelf (COTS) OFDM transmitters (as those used in Wi-Fi) in large-scale deployment.

In our setup, we use a low-cost SDR, the BladeRF 2.0 Micro [37], to generate the multi-tone BPSK signal. The BladeRF is configured to output -5dBm, which is then amplified by a QPA9908 Power Amplifier (PA) [40] with a gain of 32.5dB. The amplified signal is transmitted through an 8.5 dBi Vulcan RFID S9028PCR (RHCP) Indoor RFID Antenna [55]. The total transmitted power is calculated as: $-5 + 32.5 + 8.5 = 36\ dBm(4\ W)$, which complies with FCC EIRP regulations.

7.2 Passive Tag

We design two custom PCB boards with COTS components as a prototype of a passive tag: the rectifier board for RF signal down-conversion, and the filter board for power, clock, data separation.

7.2.1 Rectifier board. The rectifier board consists of two main components: the Impedance Matching Network (IMN) and a Dickson rectifier. We use a small form-factor TE Connectivity monopole ANT-916-CW-RAH antenna (850–970MHz, 2 dBi) [50] to capture the UHF wireless signal. A 2.7 pF shunt capacitor followed by a 15 nH series inductor forms the IMN, matching the 50 Ω antenna impedance to the input impedance of the diode rectifier. We select the Skyworks SMS7630-005LF Schottky diode [48] for its low barrier voltage, a widely used choice in wireless energy harvesting platforms like WISP [59]. A 33 pF capacitor in series before the diode package and a same shunt capacitor after it forms a Dickson voltage multiplier, allowing full-wave rectification and effectively doubling the output voltage.

7.2.2 Filter board. The filter system is designed using Keysight Advanced Design System (ADS) simulations. It consists of three components: a DC LPF, a 1MHz BPF for extracting BPSK data and passively converting it to ASK, and a 2 MHz BPF for extracting the clock signal. The DC LPF includes a series LPS4018-683MRC 68μH inductor followed by a 33nF shunt capacitor. The output is connected either to an 18 kΩ load resistor for power measurement or to a BQ25570 PMU [51] for evaluating cold-start time. The 1 MHz BPF consists of a 1812FS-393JLC 39 uH series inductor followed by a 620 pF series capacitor, and then a 1812FS-152JLC 1.5 uH shunt inductor as well as a 15 nF shunt capacitor. The 2 MHz BPF consists of a 1812LS-273JLC 27 uH series inductor followed by a 240 pF capacitor, and then a 0805LS-681XJLC 680 nH shunt inductor as well as a 10 nF shunt capacitor. This design ensures efficient power extraction while preserving accurate clock and data signal recovery.

The tag's analog front end is constructed entirely from passive components, with the discrete rectifier and filter system costing approximately $0.70 at large-scale production. The design can be made even more compact and cost-effective through chip-level integration.

8 EVALUATION

We conduct extensive experiments to evaluate *3in1* across various scenarios, including multi-tone configurations, input power levels, channel fading, cold-start time, and operating range. Unless stated otherwise, the default experimental setup is as follows: the input power at the receiver is -10 dBm, the load resistance for DC power is 18 kΩ, the BPSK bit rate is 200 kbps, and frequency hopping is enabled. For measurements, we utilize the Keysight Fieldfox N9952B Microwave Analyzer [32], functioning as both a spectrum and vector network analyzer, alongside the Keysight 34465A digital multimeter [31] and the Siglent SDS2354X Plus 350 MHz digital oscilloscope [47] for baseband performance analysis. The experimental setup is shown in Fig. 14.

8.1 Justification of Design Choices

8.1.1 Frequency hopping and FCC compliance. We first measure the signal strength using Keysight FieldFox N9952B with a 3 kHz resolution bandwidth for three signal types: a single-tone signal, a 16-tone non-hopping signal, and a 16-tone hopping signal, all with the same average power. To protect the equipment, the PA output is attenuated by 12 dB before connecting to the spectrum analyzer.

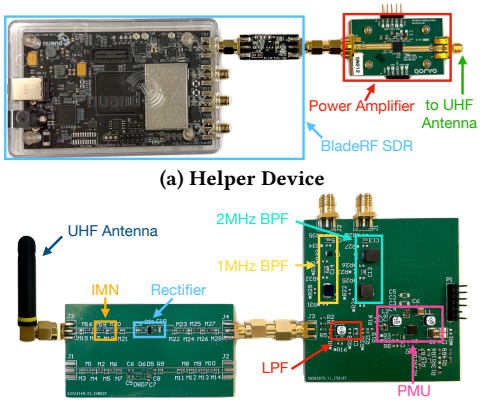

(a) Helper Device

(b) Passive Tag

Figure 13: *3IN1* Prototype

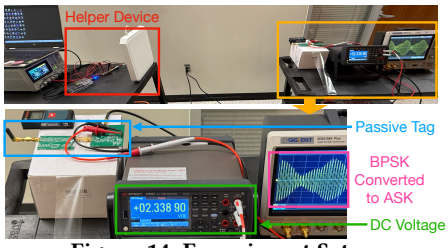

Figure 14: Experiment Setup

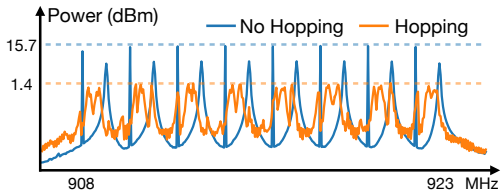

Figure 15: Power Spectrum of Hopping and Non-Hopping 16-Tone BPSK Waveforms

Peak power. By setting the resolution bandwidth to 3 kHz, we record the maximum peak power within the UHF ISM band. The results show that while the single-tone signal concentrates most of its power at one peak, reaching 28.3 dBm, the 16-tone non-hopping signal distributes its power more evenly, reducing the peak power to 15.7 dBm— still exceeding the 8 dBm FCC regulation limit. As shown in Fig. 15, with frequency hopping enabled, the peak channel power is further reduced to 1.4 dBm, well below the 8 dBm upper bound, ensuring FCC compliance.

Impact on power, clock and data performance. We assess whether frequency hopping adversely affects power delivery, clock stability, or data communication. Two 16-tone signals—one with hopping and one without—are generated with identical average power (-10 dBm) and fed into our tag prototype through cable. Measurements of the extracted 2 MHz clock voltage, clock jitter, and 1 MHz downlink Bit Error Rate (BER) reveal no significant differences in DC voltage, clock voltage, or jitter (consistently below 1 ns) between the two cases, as shown in Fig. 17. Furthermore, the BER remains stable at 10^{-4} across all configurations, demonstrating that frequency hopping preserves power, clock, and data integrity while enabling regulatory compliance.

8.1.2 Multi-tone BPSK modulation. To validate that our multi-tone BPSK modulation design does not affect power or clock delivery, we compare two 16-tone signals with identical average power (-10 dBm)—one with BPSK modulation applied to half of the tones and the other without modulation. As illustrated in Fig. 17, the extracted DC voltage and clock voltage show no significant differences between the two signals, and the clock jitter remains consistently below 1 ns. These results demonstrate that multi-tone BPSK modulation preserves power delivery and maintains wireless clocking integrity without distortion.

8.2 Impact of Input Power and Tone Number

The received power at a battery-free tag is a critical factor influencing power harvesting efficiency, as higher received power generally improves power conversion efficiency (PCE) due to the threshold voltage of diode rectifiers. In this section, we analyze the impact of received power and the number of tones on power, clock, and data delivery. The experiments are conducted by first calibrating the transmit power using the Keysight FieldFox N9952B and then feeding the signal to the passive tag board via a cable. This setup ensures precise control over input power levels and accurate measurement of the system's performance under varying conditions.

8.2.1 Harvested power. We investigate the effect of the number of tones on power delivery across varying input power levels. Waveforms with 1, 2, 4, 8, and 16 tones, as well as an emulated Gen2 UHF RFID protocol waveform (single-tone with ASK modulation), are generated with the same average power. The input power at the receiver is varied from -30 dBm to 0 dBm, and the harvested power after rectification is recorded. Results are shown in Fig. 16, where the left y-axis represents harvested power and the right y-axis shows the relative gain compared to the Gen2 UHF RFID protocol.

As illustrated in Fig. 16, harvested power increases monotonically with the number of tones across all input power levels. The Gen2 configuration exhibits the lowest harvested power due to the impact of ASK modulation on average power. Compared to Gen2, *3IN1* with 16 tones achieves over 6x gain at -20 dBm input power and over 5x gain at -10 dBm and -30 dBm input power, demonstrating the superiority of the multi-tone approach in power harvesting efficiency.

8.2.2 Power conversion efficiency. PCE is another critical metric for assessing the effectiveness of a power harvesting circuit design. We measure the PCE of our receiver across different input power levels and waveform configurations, including varying numbers of tones in *3IN1* and a Gen2 waveform as the baseline. As illustrated in Fig. 18, PCE improves monotonically with both an increasing number of tones and higher input power. This trend aligns with the expected behavior of Schottky diodes, which exhibit higher PCE at elevated input power levels.

The measured PCE reaches a maximum of 61.2% at 0 dBm input power with a 16-tone signal, while the Gen2 signal achieves only 15% PCE under the same conditions. Furthermore, the PCE gain of the 16-tone configuration over Gen2 exceeds 5x for input power levels at or below -5 dBm, demonstrating significant improvements

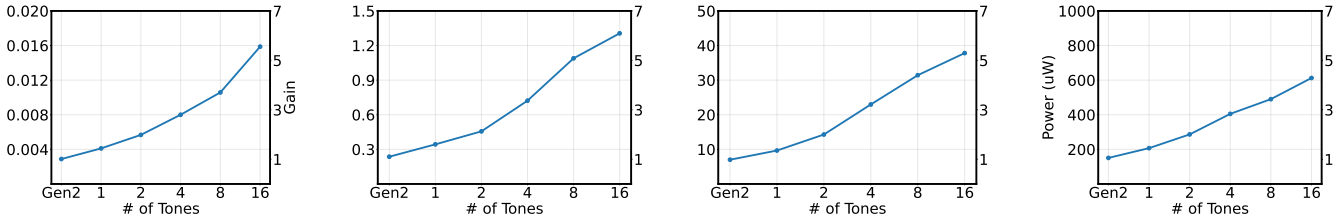

(a) -30 dBm (b) -20 dBm (c) -10 dBm (d) 0 dBm

Figure 16: Received Power v.s. Gen2 UHF RFID Protocol and # of Tones of *3in1*

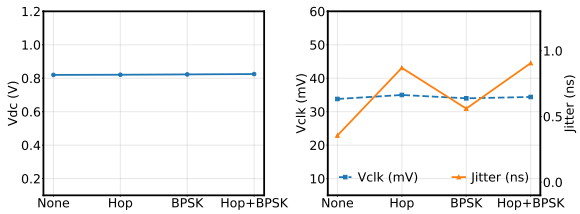

(a) Power (b) Clock voltage and jitter

Figure 17: V_{DC}, V_{CLK} and Clock Jitter v.s. BPSK and Hopping at -10 dBm Input Power

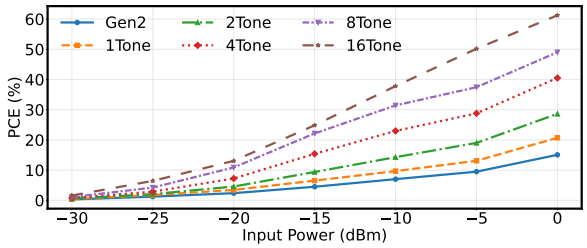

Figure 18: Power Conversion Efficiency v.s. Input Power and Number of Tones

in both efficiency and sensitivity compared to state-of-the-art systems. These results underscore the effectiveness of our multi-tone approach in enhancing power harvesting performance.

8.2.3 Clock and data delivery. We evaluate clock and data delivery performance by generating a 16-tone waveform with frequency hopping and BPSK modulation at varying power levels. The BladeRF output is fed into our tag prototype, and we measure the extracted clock voltage and clock jitter after the 2 MHz BPF, as well as the bit error rate (BER) of downlink communication at 200 kbps after the 1 MHz BPF.

As shown in Fig. 20a, the clock voltage increases with higher input power, while clock jitter shows a slight downward trend, consistent with the expected improvement in SNR at higher power levels. The maximum clock jitter observed is 1.09 ns at -30 dBm, while jitter remains below 1 ns at all other power levels. Similarly, Fig. 20b demonstrates robust data delivery, with BER staying below 10^{-4} (bounded by the number of bits we collected) for input power levels of -20 dBm and above, and remaining below 10^{-2} even at -30 dBm. These results confirm the effectiveness of our design in delivering stable clock signals and reliable data communication, even under low received power conditions. It is important to note that at lower input power levels, the harvested power becomes insufficient to sustain the functionality of passive IoT systems. As a result, the performance of clock and data communication under such conditions is less critical, as the system is unlikely to operate

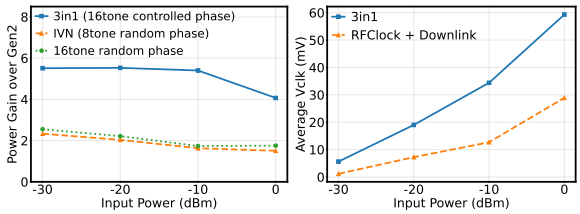

(a) Power (b) Clock

Figure 19: Comparison with SOTA

effectively. The primary focus, therefore, remains on ensuring robust performance at power levels where the system is operational, as demonstrated by the results at -30 dBm and above.

8.2.4 Comparison with SOTA. Since no prior work integrates powering, clocking, and downlink communication into a single optimized system, a direct one-to-one comparison is not feasible. We therefore evaluate the performance of *3in1* against state-of-the-art (SOTA) systems by comparing the key functionalities that represent the primary bottlenecks in passive IoT: wireless powering and clocking.

For wireless powering, we compare our 16-tone, controlled-phase waveform against the 8-tone, random-phase waveform used by IVN [33]. To clearly isolate the benefits of our phase control, we also include an intermediate 16-tone random-phase design in the comparison. As shown in Fig. 19a, *3in1* outperforms IVN at all input power levels, achieving a gain ranging from 2.4× to 3.3×. Notably, the 16-tone random-phase waveform yields negligible improvement over the 8-tone version, confirming that the performance gain stems not simply from the number of tones but from our careful phase control, which optimizes the waveform's PAPR.

For wireless clocking, we compare *3in1* to RFClock [2], which uses a 2-tone signal. To ensure a fair comparison, we modify the RFClock waveform to incorporate a BPSK downlink, mirroring the multifunctionality of our system. The results in Fig. 19b demonstrate that the average extracted clock voltage of *3in1* is substantially higher, with a gain of 2.1× to 5.0× across all power levels. This improvement is attributable to our system co-design; without it, the downlink signal inevitably distorts the clock tones in the modified RFClock waveform, resulting in a lower clock voltage after band-pass filtering.

8.3 Real World Performance

We evaluate the system's performance in real-world scenarios, including operating range, PMU cold-start time, Non-Line-of-Sight (NLOS) conditions, and deep fading environments.

8.3.1 Range improvement. To evaluate the real-world indoor performance of *3in1*, we conduct an over-the-air test in a building

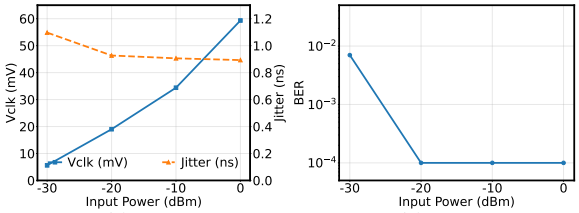

(a) Clock (b) Data

Figure 20: V_{CLK}, Clock Jitter, and BER v.s. Input Power

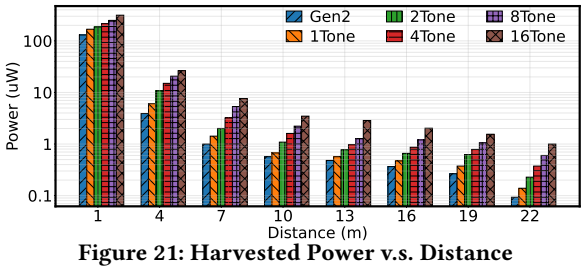

Figure 21: Harvested Power v.s. Distance

corridor to determine its maximum operating range. The distance between the prototype tag and the transmitter is varied from 1 m to 22 m in 3 m increments, while all other parameters remain unchanged. At each distance, we measure the harvested power, clock voltage, clock jitter, and BER.

As shown in Fig. 21, a higher number of tones consistently results in greater harvested power, with the Gen2 waveform yielding the lowest power at all distances. Specifically, at 22 m, the 16-tone signal enables the tag to harvest 1 μW, while the Gen2 waveform harvests only 0.1 μW—a 10× improvement. To achieve the same harvested power as the 16-tone signal at 22 m, the Gen2 setup would need to operate within a maximum range of 7 m, which demonstrates a 3× gain on operating range. Similarly, the distances at which *3IN1* can harvest 1.5 uW and 3 uW are 19 m and 13 m, respectively; for Gen2, they are 7 m and 4 m, corresponding to 2.7× and 3.25× improvements. Given that passive RFID tags consume only 0.6 uW [39], the power harvested by *3IN1* even at 22 m is sufficient to operate such tags, either continuously or with a practical charge-operate duty cycle.

Fig. 22a shows that while the clock voltage decreases with increasing distance, the clock jitter remains stable. The maximum clock jitter is 1.08 ns at 22 m, while at shorter distances, it remains below 1 ns, well within the acceptable range for passive IoT devices. The BER results, presented in Fig. 22b, indicate that BER stays below 10^{-4} within 19 m and remains below 10^{-3} even at 22 m. These results demonstrate that *3IN1* significantly extends the operating range of passive IoT systems while maintaining reliable power, clock, and data delivery, making it highly suitable for real-world applications.

8.3.2 PMU cold-start time. The efficiency of a PMU is highly dependent on the input DC voltage level, and PMUs typically require a minimum input voltage for cold start [51]. Cold-start time is a critical parameter for evaluating the power harvesting efficiency of battery-free tags, as long cold-start times remain a significant barrier to their widespread deployment. To assess this, we measure the time required for the PMU's DC output to stabilize at 1.3 V, a suitable voltage level for low-power microcontrollers (MCUs) and peripheral circuits [4].

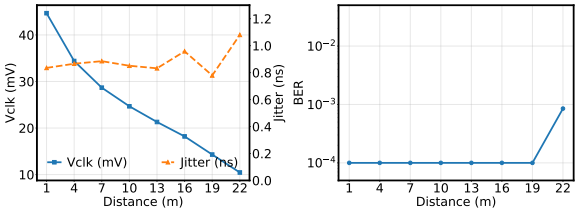

(a) Clock (b) Data

Figure 22: V_{CLK}, Clock Jitter, and BER v.s. Distance

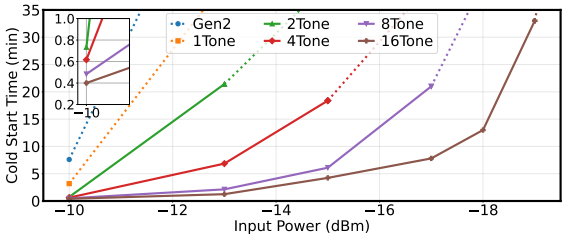

Figure 23: PMU Cold Start Time v.s. Input Power

As shown in Fig. 23, the number of tones significantly impacts the cold-start time. With more tones, the PMU can cold-start at lower input power levels. For a 16-tone signal, the PMU can cold-start with as little as -19 dBm input power, whereas a 1-tone or Gen2 signal requires at least -10 dBm to initiate the process. At -10 dBm input power, the Gen2 signal takes 7.6 minutes to cold-start the PMU, while the 16-tone signal achieves the same in just 24 seconds—a 19x improvement. This dramatic reduction in cold-start time demonstrates the superior efficiency of *3IN1* and opens the door to new application scenarios for battery-free devices.

8.3.3 Non-line-of-sight. We evaluate the performance of *3IN1* under three Non-Line-of-Sight (NLOS) scenarios, each with a different type of blocking material between the tag and the transmitter: (i) a 3 cm thick wooden door, (ii) a 1 cm thick glass window, and (iii) glass window combined with aluminum blinds, as illustrated in Fig. 24a. The tag is placed at distances of 5 m and 10 m from the transmitter. As shown in Fig. 25, across all blocking materials, the *3IN1* tag consistently harvests significantly more power than the Gen2 baseline, with gains ranging from 6.2× to 14.4×. Meanwhile, the wireless clocking jitter remains around 1 ns, and the downlink BER stays near 10^{-4}. These results demonstrate the robustness and superior performance of *3IN1* compared to the baseline in real-world NLOS environments.

8.3.4 Deep fading. We evaluate the performance of *3IN1* under deep fading conditions by placing the tag at five locations within an office environment: (i) near a computer monitor, (ii) near aluminum blinds, (iii) near a wooden door, (iv) under a metal cabinet, and (v) behind stacks of paper boxes, as shown in Fig. 24b. The transmitter is positioned 5 m away from the tag. Due to space constraints, we reduce the transmit power by 5 dB to emulate a longer-range scenario. As shown in Fig. 26, despite the presence of strong reflectors causing deep fading, *3IN1* consistently achieves a power harvesting gain of 7.1× to 36× over the Gen2 baseline. Moreover, the wireless clocking jitter remains below 1 ns, and the downlink BER stays under 10^{-4} across all five locations, demonstrating the robustness of *3IN1* in challenging multipath-rich environments.

(a) NLOS (b) Deep Fading

Figure 24: NLOS and Deep Fading Experiment Setup

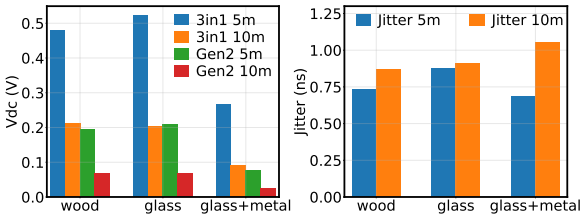

(a) Power (b) Clock and Data

Figure 25: NLOS Performance with 3 Blocking Materials

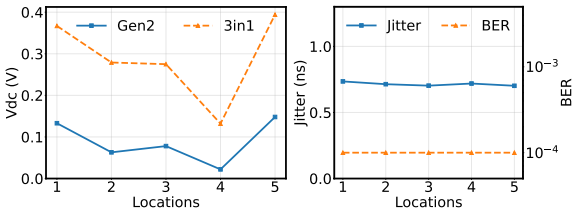

(a) Power (b) Clock and Data

Figure 26: Power, Clock Jitter and BER at 5 Fading Locations

9 DISCUSSION

Uplink Desgin. While *3in1* primarily addresses the downlink bottleneck in passive IoT systems, existing uplink designs can be readily integrated into our architecture. With wireless clocking enabled by *3in1*, frequency-shifting backscatter communication [61] can leverage the precise clock to enhance performance, making it a natural complement to our design. Alternatively, Impulse Radio Ultra-Wideband (IR-UWB) [43] offers a promising solution, enabling low-power, high-data-rate communication without requiring carrier generation. A clock amplification stage, as demonstrated in prior works [1, 2], can be readily incorporated for uplink modulation. Additionally, harmonic components generated by multi-tone self-mixing in the rectifier stage may serve as potential carriers for the uplink.

Integration with Beamforming. While our approach focuses on single-antenna multi-tone waveform optimization for efficient power, clock, and data delivery, it is orthogonal to beamforming techniques. In fact, beamforming could complement our system by further extending the operating range. Inspired by prior work [57], multiple helper devices could be deployed to perform collaborative beamforming, directing power towards tags more efficiently. Such an approach could mitigate spatial inefficiencies and improve power availability in challenging environments.

Scalability and Concurrent Operation. A key advantage of our system is its inherent scalability. Our approach enables simultaneous downlink power, clock, and data delivery to an arbitrary number of tags. Since the powering and clocking signals are broadcast globally, they are inherently available to all tags simultaneously. For the downlink, multiple access can be achieved using a straightforward Time-Division Multiple Access (TDMA) scheme, drawing a parallel to established protocols like EPC Gen2 RFID. Since different tags may operate asynchronously—some in a sleep state, some receiving downlink communication, and others transmitting uplink signals—this allows for efficient time-multiplexed operation without requiring strict synchronization. This flexibility is particularly beneficial in large-scale passive IoT deployments, where dynamic power demands and communication patterns vary across tags.

Security and Privacy. The proposed 16-tone design, combined with frequency hopping, provides inherent robustness against jamming attacks. This resilience is achieved through a self-mixing mechanism; even if a subset of tones is compromised by a jammer, the remaining uncorrupted tones are sufficient to generate the necessary clock and downlink signals. A notable side-effect of this architecture is that a strong jamming signal, rather than disabling the system, can paradoxically enhance its power harvesting performance by increasing the available RF energy for scavenging.

Regarding security, privacy is maintained as the powering and clocking signals contain no user data, preventing information leakage through these channels. For the downlink data channel, standard encryption techniques can be readily applied in sensitive environments. This allows for a flexible security model, though it necessitates a trade-off between the computational overhead of encryption and the desired level of data confidentiality.

Future Work. Several avenues remain open for future exploration. First, refining the uplink strategy by evaluating the energy-efficiency and reliability of different backscatter and IR-UWB implementations will be critical. Second, the integration of beamforming with multi-tone WPT could enhance both range and efficiency, warranting further study. Third, integrating a wireless sensing modality to create a *4in1* system is an opportunity for future research. Lastly, investigating advanced scheduling mechanisms to dynamically allocate power and communication resources based on tag priority and application needs will be essential for scaling the system in real-world deployments.

10 CONCLUSION

We present *3in1*, a novel multi-tone system that jointly optimizes wireless power delivery, high-precision clocking, and robust communication to overcome key limitations of passive IoT technology. By leveraging high-PAPR multi-tone signals and carefully controlling its phase modulation and frequency spacing, *3in1* enhances energy harvesting, enables wireless clocking, and ensures robust downlink communication without disrupting power transfer. We implement *3in1* using a software-defined radio (SDR)-based transmitter and a custom-built passive tag. Real-world experiments demonstrates significant performance gains, including a 6× improvement in power conversion efficiency, 3× increase in operating range (up to 22 m), and 19× faster cold-start time compared to the Gen2 UHF RFID protocol. Simultaneously, *3in1* delivers a clock signal with zero offset at 2 MHz and < 1 ns jitter, along with a high-speed 200 kbps downlink achieving a bit error rate (BER) below 10^{-3}—all while remaining fully compliant with FCC regulations. These results highlight *3in1* as a major advancement toward efficient, long-range passive IoT deployment in real-world applications.

References

[1] Omid Abari, Hariharan Rahul, Dina Katabi, and Mondira Pant. 2015. AirShare: Distributed coherent transmission made seamless. In *2015 IEEE Conference on Computer Communications (INFOCOM)*. IEEE, 1742–1750.

[2] Kubra Alemdar, Divashree Varshney, Subhramoy Mohanti, Ufuk Muncuk, and Kaushik Chowdhury. 2021. RFClock: Timing, phase and frequency synchronization for distributed wireless networks. In *Proceedings of the 27th Annual International Conference on Mobile Computing and Networking*. 15–27.

[3] Zhenlin An, Qiongzheng Lin, Qingrui Pan, and Lei Yang. 2021. Turbocharging deep backscatter through constructive power surges with a single RF source. In *IEEE INFOCOM 2021-IEEE Conference on Computer Communications*. IEEE, 1–10.

[4] Analog Devices. [n. d.]. MAX32670. https://www.analog.com/media/en/technical-documentation/data-sheets/max32670-max32671.pdf.

[5] Farzad Asgarian and Amir M Sodagar. 2009. A low-power noncoherent BPSK demodulator and clock recovery circuit for high-data-rate biomedical applications. In *2009 Annual International Conference of the IEEE Engineering in Medicine and Biology Society*. IEEE, 4840–4843.

[6] Aloÿs Augustin, Jiazi Yi, Thomas Clausen, and William Mark Townsley. 2016. A study of LoRa: Long range & low power networks for the internet of things. *Sensors* 16, 9 (2016), 1466.

[7] Majid Baghaei-Nejad, Hannu Tenhunen, and Li-Rong Zheng. 2007. Power management and clock generator for a novel passive UWB tag. In *2007 International Symposium on System-on-Chip*. IEEE, 1–4.

[8] Raymond E Barnett, Jin Liu, and Steve Lazar. 2009. A RF to DC voltage conversion model for multi-stage rectifiers in UHF RFID transponders. *IEEE Journal of solid-state circuits* 44, 2 (2009), 354–370.

[9] B Beheshti and M Jalali. 2012. A low-power noncoherent BPSK demodulator for implantable medical devices. In *2012 IEEE International Conference on Electronics Design, Systems and Applications (ICEDSA)*. IEEE, 203–206.

[10] Dinesh Bharadia, Kiran Raj Joshi, Manikanta Kotaru, and Sachin Katti. 2015. Backfi: High throughput wifi backscatter. *ACM SIGCOMM Computer Communication Review* 45, 4 (2015), 283–296.

[11] Alirio Boaventura, Daniel Belo, Ricardo Fernandes, Ana Collado, Apostolos Georgiadis, and Nuno Borges Carvalho. 2015. Boosting the efficiency: Unconventional waveform design for efficient wireless power transfer. *IEEE Microwave Magazine* 16, 3 (2015), 87–96.

[12] Alírio J Soares Boaventura and Nuno Carvalho. 2012. Extending reading range of commercial RFID readers. *IEEE Transactions on Microwave Theory and Techniques* 61, 1 (2012), 633–640.

[13] Alírio Soares Boaventura and Nuno Borges Carvalho. 2011. Maximizing DC power in energy harvesting circuits using multisine excitation. In *2011 IEEE MTT-S International Microwave Symposium*. IEEE, 1–4.

[14] Alírio Soares Boaventura and Nuno Borges Carvalho. 2012. Enhanced front-end to extend reading range of commercial RFID readers using efficient multisine signals. In *2012 IEEE/MTT-S International Microwave Symposium Digest*. IEEE, 1–3.

[15] Ferran Bolos, Javier Blanco, Ana Collado, and Apostolos Georgiadis. 2016. RF Energy Harvesting From Multi-Tone and Digitally Modulated Signals. 64, 6 (2016), 1918–1927. doi:10.1109/TMTT.2016.2561923

[16] Nuno B Carvalho, Kate A Remley, Dominique Schreurs, and Kevin G Gard. 2008. Multisine signals for wireless system test and design [application notes]. *IEEE Microwave Magazine* 9, 3 (2008), 122–138.

[17] Bruno Clerckx and Ekaterina Bayguzina. 2016. Waveform design for wireless power transfer. *IEEE Transactions on Signal Processing* 64, 23 (2016), 6313–6328.

[18] A. Collado and A. Georgiadis. 2014. Optimal Waveforms for Efficient Wireless Power Transmission. 24, 5 (2014), 354–356. doi:10.1109/LMWC.2014.2309074

[19] Shilpa Devalal and A Karthikeyan. 2018. LoRa technology-an overview. In *2018 second international conference on electronics, communication and aerospace technology (ICECA)*. IEEE, 284–290.

[20] Manideep Dunna, Miao Meng, Po-Han Wang, Chi Zhang, Patrick Mercier, and Dinesh Bharadia. 2021. {SyncScatter}: Enabling {WiFi} like synchronization and range for {WiFi} backscatter communication. In *18th USENIX symposium on networked systems design and implementation (NSDI 21)*. 923–937.

[21] Xiaoran Fan, Longfei Shangguan, Richard Howard, Yanyong Zhang, Yao Peng, Jie Xiong, Yunfei Ma, and Xiang-Yang Li. 2020. Towards flexible wireless charging for medical implants using distributed antenna system. In *Proceedings of the 26th annual international conference on mobile computing and networking*. 1–15.

[22] FCC. [n. d.]. FCC 47 CFR 15.247. https://www.ecfr.gov/current/title-47/chapter-I/subchapter-A/part-15/subpart-C/subject-group-ECFR2f2e5828339709e/section-15.247.

[23] Milad Ghazi, Mohammad Hossein Maghami, Parviz Amiri, and Sotoudeh Hamedi-Hagh. 2020. An Ultra-Low-Power Area-Efficient Non-Coherent Binary Phase-Shift Keying Demodulator for Implantable Biomedical Microsystems. *Electronics* 9, 7 (2020), 1123.

[24] GSMA. [n. d.]. 5G Advanced to Support Self-Powered Sensors. https://www.gsma.com/5ghub/iot.

[25] Xiuzhen Guo, Longfei Shangguan, Yuan He, Nan Jing, Jiacheng Zhang, Haotian Jiang, and Yunhao Liu. 2022. Saiyan: Design and implementation of a low-power demodulator for {LoRa} backscatter systems. In *19th USENIX Symposium on Networked Systems Design and Implementation (NSDI 22)*. 437–451.

[26] Khodr Hammoud, Sofie Pollin, and Dominique Schreurs. 2022. Efficient Indoor Solar Panel Energy Harvesting Exploiting the Crest Factor. In *2022 Wireless Power Week (WPW)* (Bordeaux, France, 2022-07-05). IEEE, 653–657. doi:10.1109/WPW54272.2022.9854033

[27] Seung Hee Han and Jae Hong Lee. 2005. An overview of peak-to-average power ratio reduction techniques for multicarrier transmission. *IEEE wireless communications* 12, 2 (2005), 56–65.

[28] Xiongchuan Huang, Ao Ba, Pieter Harpe, Guido Dolmans, Harmke de Groot, and John R Long. 2012. A 915 MHz, ultra-low power 2-tone transceiver with enhanced interference resilience. *IEEE journal of solid-state circuits* 47, 12 (2012), 3197–3207.

[29] Impinj. [n. d.]. xSpan Gateway RFID Reader. https://rfid.atlasrfidstore.com/hubfs/1_Tech_Spec_Sheets/Impinj/ATLAS%20Impinj%20xSpan%20Gateway%20RFID%20Reader%20Version%202.1.pdf.

[30] Bryce Kellogg, Vamsi Talla, Shyamnath Gollakota, and Joshua R Smith. 2016. Passive {Wi-Fi}: Bringing Low Power to {Wi-Fi} Transmissions. In *13th USENIX Symposium on Networked Systems Design and Implementation (NSDI 16)*. 151–164.

[31] Keysight. 2026. 34465A. https://www.keysight.com/us/en/product/34465A/digital-multimeter-6-5-digit-truevolt-dmm.html.

[32] Keysight. 2026. N9952B. https://www.keysight.com/us/en/product/N9952B/field-fox-b-handheld-microwave-analyzer-50-ghz.html.

[33] Yunfei Ma, Zhihong Luo, Christoph Steiger, Giovanni Traverso, and Fadel Adib. 2018. Enabling deep-tissue networking for miniature medical devices. In *Proceedings of the 2018 Conference of the ACM Special Interest Group on Data Communication*. 417–431.

[34] Jesse Moody, Pouyan Bassirian, Abhishek Roy, Ningxi Liu, N Scott Barker, Benton H Calhoun, and Steven M Bowers. 2019. Interference robust detector-first near-zero power wake-up receiver. *IEEE Journal of Solid-State Circuits* 54, 8 (2019), 2149–2162.

[35] Jesse Moody, Anjana Dissanayake, Henry Bishop, Ruochen Lu, Ningxi Liu, Divya Duvvuri, Anming Gao, Daniel Truesdell, N Scott Barker, Songbin Gong, et al. 2019. A-106dBm 33nW bit-level duty-cycled tuned RF wake-up receiver. In *2019 symposium on VLSI Circuits*. IEEE, C86–C87.

[36] Kyriakos Neophytou and MA Antoniades. 2020. High PAPR Multi-Tone Waveforms as a Method of Boosting DC voltage in RF Wireless Power Transfer Systems. In *2020 14th European Conference on Antennas and Propagation (EuCAP)*. IEEE, 1–4.

[37] Nuand. [n. d.]. BladeRF 2.0 Micro. https://www.nuand.com/bladerf-2-0-micro/.

[38] Mahmoud H. Ouda, Paul Mitcheson, and Bruno Clerckx. 2018. Optimal Operation of Multitone Waveforms in Low RF-Power Receivers. In *2018 IEEE Wireless Power Transfer Conference (WPTC)* (Montreal, QC, Canada, 2018-06). IEEE, 1–4. doi:10.1109/WPT.2018.8639426

[39] Vijay Pillai, Harley Heinrich, David Dieska, Pavel V Nikitin, Rene Martinez, and KV Seshagiri Rao. 2007. An ultra-low-power long range battery/passive RFID tag for UHF and microwave bands with a current consumption of 700 nA at 1.5 V. *IEEE Transactions on Circuits and Systems I: Regular Papers* 54, 7 (2007), 1500–1512.

[40] Qorvo. [n. d.]. QPA9908. https://www.qorvo.com/products/p/QPA9908.

[41] Mohammad Rostami, Xingda Chen, Yuda Feng, Karthikeyan Sundaresan, and Deepak Ganesan. 2021. MIXIQ: Re-thinking ultra-low power receiver design for next-generation on-body applications. In *Proceedings of the 27th annual international conference on mobile computing and networking*. 364–377.

[42] Mohammad Rostami and Karthikeyan Sundaresan. 2022. Enabling high accuracy pervasive tracking with ultra low power uwb tags. In *Proceedings of the 28th Annual International Conference on Mobile Computing And Networking*. 459–472.

[43] Mohammad Rostami and Karthikeyan Sundaresan. 2022. Enabling high accuracy pervasive tracking with ultra low power UWB tags. In *Proceedings of the 28th Annual International Conference on Mobile Computing And Networking* (Sydney, NSW, Australia) *(MobiCom '22)*. Association for Computing Machinery, New York, NY, USA, 459–472. doi:10.1145/3495243.3560542

[44] Mohammad Rostami, Karthik Sundaresan, Eugene Chai, Sampath Rangarajan, and Deepak Ganesan. 2020. Redefining passive in backscattering with commodity devices. In *Proceedings of the 26th Annual International Conference on Mobile Computing and Networking*. 1–13.

[45] Stefan Schmickl, Thomas Faseth, and Harald Pretl. 2020. An RF-energy harvester and IR-UWB transmitter for ultra-low-power battery-less biosensors. *IEEE Transactions on Circuits and Systems I: Regular Papers* 67, 5 (2020), 1459–1468.

[46] Negin Shariati, James R. Scott, Dominique Schreurs, and Kamran Ghorbani. 2018. Multitone Excitation Analysis in RF Energy Harvesters—Considerations and Limitations. 5, 4 (2018), 2804–2816. doi:10.1109/JIOT.2018.2828978

[47] Siglent. [n. d.]. SDS2354X Plus. https://siglentna.com/product/sds2354x-plus/.

[48] Skyworks. [n. d.]. SMS7630-005LF. https://d1ehax0mqsd4rz.cloudfront.net/-/media/SkyWorks/Documents/Products/201-300/Surface-Mount-Schottky-Diodes_200041AH.pdf.

[49] Vamsi Talla, Mehrdad Hessar, Bryce Kellogg, Ali Najafi, Joshua R Smith, and Shyamnath Gollakota. 2017. Lora backscatter: Enabling the vision of ubiquitous connectivity. *Proceedings of the ACM on interactive, mobile, wearable and ubiquitous technologies* 1, 3 (2017), 1–24.

[50] TE Connectivity. [n. d.]. ANT-916-CW-RAH. https://www.te.com/en/product-ANT-916-CW-RAH.html.

[51] Texas Instruments. [n. d.]. BQ25570. https://www.ti.com/product/BQ25570.

[52] Matthew S Trotter and Gregory D Durgin. 2010. Survey of range improvement of commercial RFID tags with power optimized waveforms. In *2010 IEEE International Conference on RFID (IEEE RFID 2010)*. IEEE, 195–202.

[53] Matthew S Trotter, Joshua D Griffin, and Gregory D Durgin. 2009. Power-optimized waveforms for improving the range and reliability of RFID systems. In *2009 IEEE International Conference on RFID*. IEEE, 80–87.

[54] Christopher R. Valenta, Marcin M. Morys, and Gregory D. Durgin. 2015. Theoretical Energy-Conversion Efficiency for Energy-Harvesting Circuits Under Power-Optimized Waveform Excitation. 63, 5 (2015), 1758–1767. doi:10.1109/TMTT.2015.2417174

[55] Vulcan. [n. d.]. Vulcan RFID S9028PCR (RHCP) Indoor RFID Antenna. https://www.atlasrfidstore.com/vulcan-rfid-s9028pcr-rhcp-indoor-rfid-antenna-fcc.

[56] Rushi J Vyas, Benjamin B Cook, Yoshihiro Kawahara, and Manos M Tentzeris. 2013. E-WEHP: A batteryless embedded sensor-platform wirelessly powered from ambient digital-TV signals. *IEEE Transactions on microwave theory and techniques* 61, 6 (2013), 2491–2505.

[57] Jingxian Wang, Junbo Zhang, Rajarshi Saha, Haojian Jin, and Swarun Kumar. 2019. Pushing the range limits of commercial passive {RFIDs}. In *16th USENIX Symposium on Networked Systems Design and Implementation (NSDI 19)*. 301–316.

[58] Ron Weinstein. 2005. RFID: a technical overview and its application to the enterprise. *IT professional* 7, 3 (2005), 27–33.

[59] WISP Wiki. [n. d.]. WISP 6. https://sites.google.com/uw.edu/wisp-wiki/wisp6.

[60] Han Yan, Jose Gabriel Macias-Montero, Atef Akhnoukh, Leo CN de Vreede, John R Long, and Joachim N Burghartz. 2011. An ultra-low-power BPSK receiver and demodulator based on injection-locked oscillators. *IEEE transactions on microwave theory and techniques* 59, 5 (2011), 1339–1349.

[61] Pengyu Zhang, Dinesh Bharadia, Kiran Joshi, and Sachin Katti. 2016. Hitchhike: Practical backscatter using commodity wifi. In *Proceedings of the 14th ACM conference on embedded network sensor systems CD-ROM*. 259–271.

[62] Renjie Zhao, Purui Wang, Yunfei Ma, Pengyu Zhang, Hongqiang Harry Liu, Xianshang Lin, Xinyu Zhang, Chenren Xu, and Ming Zhang. 2020. Nfc+ breaking nfc networking limits through resonance engineering. In *Proceedings of the Annual conference of the ACM Special Interest Group on Data Communication on the applications, technologies, architectures, and protocols for computer communication*. 694–707.

[63] Renjie Zhao, Fengyuan Zhu, Yuda Feng, Siyuan Peng, Xiaohua Tian, Hui Yu, and Xinbing Wang. 2019. OFDMA-Enabled Wi-Fi Backscatter. In *The 25th Annual International Conference on Mobile Computing and Networking* (Los Cabos, Mexico) *(MobiCom '19)*. Association for Computing Machinery, New York, NY, USA, Article 20, 15 pages. doi:10.1145/3300061.3300121

[64] Fengyuan Zhu, Luwei Feng, Meng Jin, Xiaohua Tian, Xinbing Wang, and Chenghu Zhou. 2022. Towards ultra-low power ofdma downlink demodulation. In *Proceedings of the 20th ACM Conference on Embedded Networked Sensor Systems*. 725–739.